J Mater Sci (2010) 45:953–960
DOI 10.1007/s10853-009-4025-3

Fabrication of sandwich-structured ZnO/reduced graphite oxide composite and its photocatalytic properties

Xiaogang Chen · Yunqiu He · Qiong Zhang · Linjiang Li · Donghu Hu · Ting Yin

Received: 4 July 2009 / Accepted: 6 November 2009 / Published online: 18 November 2009

Abstract ZnO/RGO (ZnO/Reduced Graphite Oxide) composites with sandwich structure (layered structure) were synthesized at relatively low temperature (60 °C) using $ZnSO_4$ and GO (Graphite Oxide) as precursors. Compared with pure ZnO, ZnO/RGO composites showed greatly enhanced-UV photocatalytic activity for the degradation of the organic dye methyl orange (MO). The structure and morphology of as-prepared samples have been characterized by X-ray diffraction (XRD), Fourier transform infrared spectroscopy (FT-IR), Field Emission Scanning Electron Microscopy (FE-SEM), etc. ZnO/RGO composites had a sandwich structure, which would be enhanced when exfoliated GO was used. During the formation the composites, GO was reduced to RGO (graphite-like carbon named as Reduced Graphite Oxide, RGO). The groups which exist in GO (such as C=O, C–O–C) disappeared or obviously weakened, while the groups similar to those in graphite (such as C=C) appeared at the same time. Photoluminescence (PL) spectra of ZnO/RGO showed a significant decline compared to that of pure ZnO, which suggests that the recombination of excited electron–hole pair (e^-–h^+) may be efficiently inhibited by the transfer of electrons to the carbon neighbor. The enhanced-photocatalytic activity for ZnO/RGO can be attributed to the migration effect of photoinduced electrons on the interface of RGO and ZnO. The photocorrosion effect of ZnO was found to be evidently suppressed according to Inductively Coupled Plasma Optical Emission Spectrometry (ICP).

X. Chen · Y. He (✉) · Q. Zhang · L. Li · D. Hu · T. Yin
School of Material Science and Engineering, Tongji University, Shanghai 200092, People's Republic of China
e-mail: heyunqiu@mail.tongji.edu.cn

X. Chen
e-mail: cxgperpetual@yahoo.com.cn

Introduction

The semiconductor photocatalysis has received much attention due to its capability of completely degrade and mineralize a wide range of pollutants at ambient temperatures and pressures, which endue it great potential application in environmental cleaning, water purification, self-cleaning, and anti-bacteria [1–4]. Although TiO_2 is the most commonly used effective photocatalyst, ZnO appears to be a suitable alternative to TiO_2 since its photodegradation mechanism has been proven to be similar to that of TiO_2 [5]. Some studies have confirmed that ZnO exhibits particularly noticeable degradation of some dyes, such as bleaching wastewater of the pulp mill [6], phenol [7], and 2-phenylphenol [8]. Furthermore, the reported optimal pH value for ZnO process is close to neutral one, whereas the optimum pH for TiO_2 mostly lies in acidic region [9]. Hence the ZnO process can be another choice for the treatment of industrial effluents.

However, the photocatalytic efficiency of ZnO is suppressed substantially due to the high recombination ratio of photoinduced electron–hole pairs (e^-–h^+). In recent years, several attempts have been made to reduce this recombination by combining photocatalyst with carbon materials, such as CNT [10] and C_{60} [11], both of which take the role of electron scavenging agents. However, neither CNT nor C_{60} is suitable to be extensively used now for their high price and complex process.

Graphite oxide (GO) that has a layered structure has attracted considerable attention in recent years [12–14]. It is obtained through the reaction of graphite with strong oxidants such as $KMnO_4$ and H_2SO_4 [15]. Polar groups (such as C=O, –C–O–C, –C–OH) appear in the interlayer of GO, which make it hydrophilic and easily hybridize with other species. These kinds of hybrid materials often exhibit

many unique physical and chemical properties [16, 17]. Besides, GO is much cheaper than CNT and C_{60}, which establish some potential applications. Recently, much attention has been focused on GO/polymers [18, 19]. However, there are few reports of GO/inorganics composites so far. Herein, we report for the first time a simple method to chemically synthesize ZnO/RGO (ZnO/reduced graphite oxide) in aqueous at relatively low temperature (60 °C).

A pH above 9.0 is essential for the formation of ZnO in aqueous solution at low temperature [20]. In the aqueous solution, soluble ions are Zn^{2+} and $ZnOH^{+}$ under acidic conditions of pH $< \sim 6.0$ [21]. With OH^{-} increasing in the aqueous solution, the precipitation of $Zn(OH)_2$ occurs under neutral and moderately basic conditions:

$$Zn^{2+} + 2OH^{-} \rightarrow Zn(OH)_2(s) \quad (1)$$

Further increase of OH^{-} causes the dissolution of $Zn(OH)_2$ and the precipitation of ZnO simultaneously because the latter's solubility is lower in higher pH region. Finally, $Zn(OH)_2$ will totally transform into ZnO through the dissolution-deposition process with an increase in pH. The reaction can be expressed as:

$$Zn(OH)_2(s) \rightarrow Zn(OH)_2(aq) \rightarrow ZnO(s) + 1/2H_2O \quad (2)$$

In the present study, a strong basic solution ($[OH^{-}]$: $[Zn^{2+}] = 20$) was applied for the preparation of wurtzite ZnO and ZnO/RGO. We found that ZnO/RGO composites have a sandwich structure, which greatly depends on the reaction process. The UV photocatalytic activity of ZnO/RGO composites showed great enhancement compared to the pure ZnO nanopowders. Moreover, we have also studied the formation process of ZnO/RGO composites, the photocatalysis mechanism of ZnO/RGO, and the photocorrosion effect of different samples.

Experimental section

Materials preparation

All the reagents were of analytic purity, bought from Sinopharm Chemical Reagent Co, Ltd (SCRC) and without further purification before utilization. High purity deionized water made ourselves was used as solvent. GO was prepared by modified Hummer method, the previous work carried out by our group [22].

Preparation of ZnO

ZnO was synthesized by simply mixing the solutions of NaOH and $ZnSO_4$ at 60 °C. 100 mL of 4 M NaOH was added drop by drop into of 100 mL of 0.2 M $ZnSO_4$ in 10 min. The reaction was performed at 60 °C for 30 min. White precipitates were obtained by filter and washing to neutral pH value with plenty of deionized water. The products were dried at 80 °C for 24 h in the air.

Preparation of D-ZnO/RGO

14 mL of GO was mixed with $ZnSO_4$ solution under stirring. After sonicating for a period of time, the solution was then transferred into a water bath (60 °C). NaOH solution was dropped in after the temperature was stable. The following steps are similar to that of pure ZnO production. The ratio ($[OH^{-}]$: $[Zn^{2+}] = 20$) was fixed in this system. This process was defined as direct synthesis method; the product was denoted as D-ZnO/RGO.

Preparation of E-ZnO/RGO

In order to form a better sandwich structure of ZnO/RGO composite, NaOH solution was tried to exfoliate GO to enlarge the interlayer distance. A colloidal solution of GO was obtained by mixing 14 mL of GO solution with 14 mL of 0.1 M NaOH aqueous solution and sonicating for 30 min. The GO colloidal solution can be named as EGO (exfoliated GO). The obtained EGO was then mixed with $ZnSO_4$ solution under vigorous stirring. After sonicating for a period of time, the solution was then transferred into a water bath (60 °C). NaOH solution was dropped in after the temperature was stable. The following steps are similar to that of pure ZnO production. The ratio ($[OH^{-}]$: $[Zn^{2+}] = 20$) was also fixed in this system. This process was defined as exfoliate synthesis method; the product was denoted as E-ZnO/RGO.

Characterization

Powder X-ray diffraction (XRD) patterns were recorded on a Rigaku D/Max-rB12KW X-ray diffractometer in the diffraction angle range $2\theta = 5$–$70°$ at a rate of 5°/min using CuKα radiation ($\lambda = 0.15418$ nm). Fourier transform infrared spectroscopy (FT-IR) was recorded on a Bruker VECTOR22 FT-IR spectrometer using KBr pellets. The morphology of the as-prepared samples was observed using a field-emission scanning electron microscope (FE-SEM, Quanta 200 FEG). The room temperature photoluminescence (PL) was measured by a 970CRT-luminescence spectrophotometer, using the 325 nm excitation line of a Xe lamp. The concentration of Zn^{2+} in the catalysts suspension was measured using Inductively Coupled Plasma Optical Emission Spectrometry (ICP, PerkinElmer, Optima 2100 DV).

Photocatalytic experiments

The photocatalytic activity of the as-prepared samples was characterized under UV light using methyl orange (MO) as a target. Experiments were as follows: 0.05 g of sample was dispersed in 50 mL of aqueous MO solution with a concentration 20 mg/L. Fresh air was bubbled for the purpose of stirring and oxygen supply. High pressure Hg lamp (250 W, $\lambda \geq 365$ nm) was used as a UV source. Suspensions were collected every 30 min to monitor the degradation of MO. The transmittance (T_i) of the centrifuged suspensions was measured at 483 nm. Absorbance (A_i) was obtained by Lambert–Beer law ($A_i = 2-\lg T_i$). And then degradation efficiency (D_i) was available according the following equation:

$$D_i = (A_0 - A_i)/A_0 \quad (3)$$

A_0 is the absorbance of MO solution at 483 nm before exposing under UV light.

In order to the investigate photostabilities of as-prepared samples, the suspensions of P-ZnO and E-ZnO/RGO were exposed under UV light for a period of time. A certain amount of suspension was withdrawn at 30, 50, and 80 h to carry the photocatalytic experiment and ICP test.

Results

XRD analysis

Figure 1a–d shows X-ray diffraction patterns for pure ZnO, D-ZnO/RGO, E-ZnO/RGO, and GO. All the peaks of as-prepared samples (Fig. 1a–c) can be indexed to the wurtzite ZnO (JCPDS card No. 36-1451). No characteristic peaks were observed for ether GO or graphite in both D-ZnO/RGO and E-ZnO/RGO. The particle sizes were estimated employing Debye–Scherrer's formula and the values were listed in Table 1. The average crystal size of ZnO in both D-ZnO/RGO and E-ZnO/RGO is slightly lower than that of pure ZnO. This can be attributed to the appearance of GO, which may suppress the growth of grains in some extent.

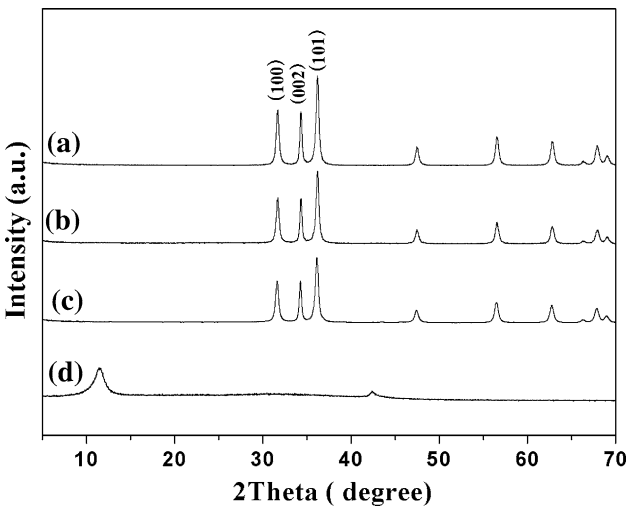

Fig. 1 XRD patterns of (*a*) pure ZnO; (*b*) D-ZnO/RGO; (*c*) E-ZnO/RGO; (*d*) graphite oxide

Table 1 Crystallite size measurement and photodegradation efficiencies

Sample	d^a (nm)	D^b (%)
Pure ZnO	26.1	28.02
D-ZnO/RGO	25.4	50.92
E-ZnO/RGO	23.4	70.3
Degussa P25	21	59.7

d^a is the crystal size calculated by plane (101), D^b is the photocatalytic efficiency at 30th min

FI-IR analysis

Figure 2 describes the FT-IR spectra of ZnO (a), D-ZnO/RGO (b), E-ZnO/RGO (c), and GO (d). In the spectrum of the pure ZnO (Fig. 2A, a), hydroxyl group vibration bands are centered at 3430 and 1620 cm^{-1}. The strong absorption band around 450 cm^{-1}corresponding to the Zn–O bonds. GO (Fig. 2A, b) exhibits the following characteristic IR features: the broad absorptions at about 3420 and 1620 cm^{-1} are assigned to the hydroxyl groups of absorbed H_2O molecules, the bands at 1720 and 1056 cm^{-1} are assigned to the C=O and C–O–C groups, respectively, the weak bands at 1390 and 1245 cm^{-1} are assigned to the O–H deformations of the C–OH groups.

As shown in Fig. 2, remarkable changes had taken place when compared D-ZnO/RGO (b) and E-ZnO/RGO (c) with GO (d). The active groups C–O–C (1056 cm^{-1}) and C=O (1720 cm^{-1}) which existed in GO disappeared or obviously weakened in both D-ZnO/RGO (b) and E-ZnO/RGO (c). The range of 1800–1400 cm^{-1} is magnified in Fig. 2B. The C=O (1720 cm^{-1}) could not be found in D-ZnO/RGO (Fig. 2B, b) while a weak band assigned to the C=C bonds appeared at 1580 cm^{-1}. It indicates that GO was reduced to graphite-like carbon (Reduced GO, RGO) during the reaction, but the graphitization degree is relatively low. Meanwhile, distinct C=C bonds (1580 cm^{-1}) presented in E-ZnO/RGO (Fig. 2B, d), suggesting a higher graphitization degree of GO. However, the weak band of C=O (1720 cm^{-1}) was observed in E-ZnO/RGO at all. The pretreatment of GO with NaOH may be responsible for this phenomenon.

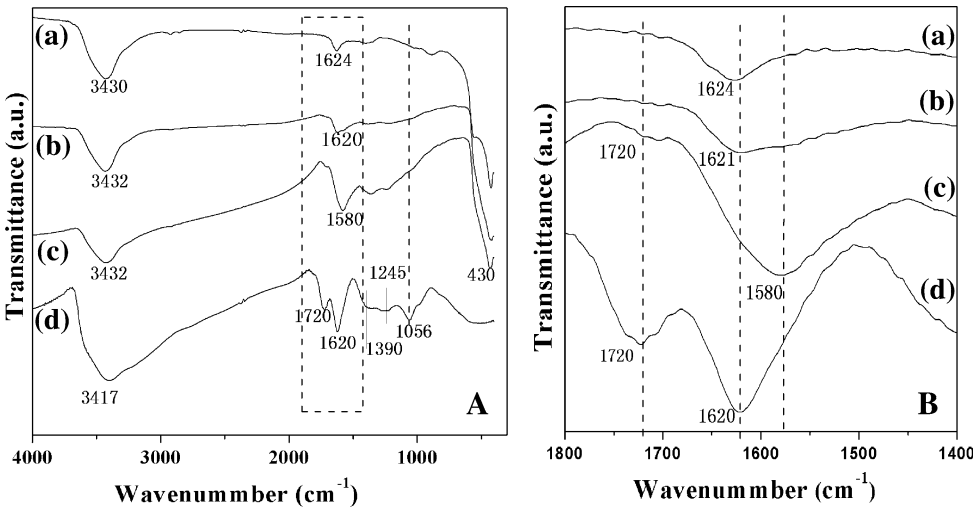

Fig. 2 FT-IR spectra of (*a*) pure ZnO (*b*) D-ZnO/RGO (*c*) E-ZnO/RGO and (*d*) graphite oxide: **A** 4000–400 cm^{-1} and **B** 1800–1400 cm^{-1} (the enlarged spectra in the rectangular area of **A**)

FE-SEM studies

The FE-SEM images of D-ZnO/RGO (a, b) and E-ZnO/RGO(c, d) are shown in Fig. 3. From the image of D-ZnO/RGO in Fig. 3a, subtle-layered structure can be observed in the rectangular area. However, the layered structure is rather non-uniform. The surface of RGO is covered by a mass of agglomerated ZnO nanoparticles. We can infer that a large quantity of ZnO nanoparticles distributes on the external surface, while only a little is grown on the brink of interlayer and the inside interlayer of RGO. Consequently, the interlayer distances will be varied and thus the layered structure is not uniform (shown in the illustration, Fig. 3a).

As for E-ZnO/RGO (Fig. 3c, d), the sample shows a very regular-layered structure (Sandwich structure) in the rectangular area (shown in the illustration). Besides, ZnO nanoparticles also appear on the inside of RGO (shown by the dashed arrow). From the horizontal cross-section of RGO layer (Fig. 3d), well-distributed ZnO nanoparticles can be observed and the size is about decade nanometers, consistent with the result of XRD. Another interesting phenomenon is the rolling tendency at the brink of RGO

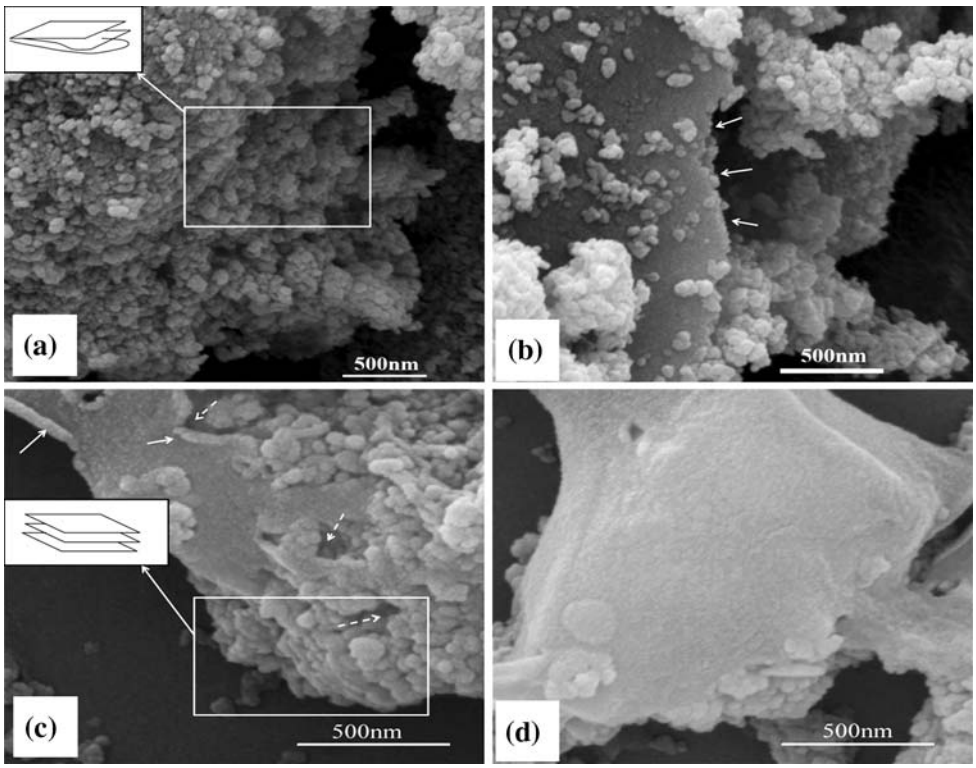

Fig. 3 FE-SEM image of D-ZnO/RGO (**a**, **b**) and E-ZnO/RGO (**c**, **d**)

layer (Fig. 3c). This may be caused by uneven stress around the layer while it is very thin. However, this rolling phenomenon does not appear in D-ZnO/RGO (Fig. 3b) because the layer not being as thin as that in E-ZnO/RGO. This may be another evidence for the formation of Sandwich structure.

The FE-SEM images reveal that the interlayer spacing is quite large by the existence of the ZnO nanoparticles, to prevent the graphite-like carbon to be observed in the XRD patterns.

Photoluminescence studies

The room temperature PL emission spectra (excitation at 325 nm) of ZnO, D-ZnO/RGO, and E-ZnO/RGO are shown in Fig. 4a–c. The spectrum for the mixture of ZnO and graphite (ZnO/graphite, Fig. 4d) is given for comparison. All samples emit strongly at the UV with a band centered at 390 nm, corresponding to the excitonic emission [23].The blue-green band around 463 nm is induced by the electron transition from the level of the ionized oxygen vacancies to the valence band [24].

Comparing to pure ZnO, the UV emission of D-ZnO/RGO (Fig. 4b) and E-ZnO/RGO (Fig. 4c) shows a significant decline indicating the decreased electron–hole pair (e^-–h^+) recombination. The reason for this may be the transfer of photo-induced electrons to RGO. E-ZnO/RGO showed even lower emission than that of D-ZnO/RGO, suggesting that the former has more evident migration effect of photo-induced electrons on the interface of RGO and ZnO.

The PL spectrum of the mixture of ZnO and graphite is slightly weaker than pure ZnO but much higher than D-ZnO/RGO and E-ZnO/RGO. So it is clear that the decline in D-ZnO/RGO and E-ZnO/RGO primarily resulted from the migration effect of photo-induced electrons instead of the absorbance of graphite.

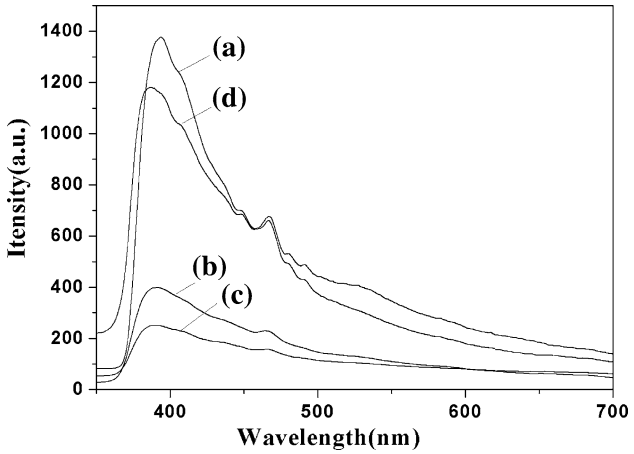

Fig. 4 PL spectrum of as-prepared samples under 325 nm UV irradiation: (*a*) Pure ZnO; (*b*) D-ZnO/RGO; (*c*) E-ZnO/RGO; (*d*) ZnO/graphite

Photocatalytic activity

The photocatalytic activities of the as-prepared samples were evaluated by the degradation of methyl orange (MO) in aqueous solution, and the results are shown in Fig. 5a. The blank test confirmed that MO was quite steady. Less than 3% of MO was degraded under UV light for 90 min in the absence of the catalyst. Meanwhile, the photocatalytic efficiency of D-ZnO/RGO and E-ZnO/RGO was much higher than that of pure ZnO. E-ZnO/RGO showed the highest activity, 70.3% of MO was degraded after exposing under UV light for 30 min. The degradation efficiencies were 50.2 and 28.0% for D-ZnO/RGO and pure ZnO, respectively. 90 min later, MO was almost completely degraded in the presence of E-ZnO/RGO and D-ZnO/RGO. However, the degradation efficiency of pure ZnO was only 61%, which was even less than the value of E-ZnO/RGO at

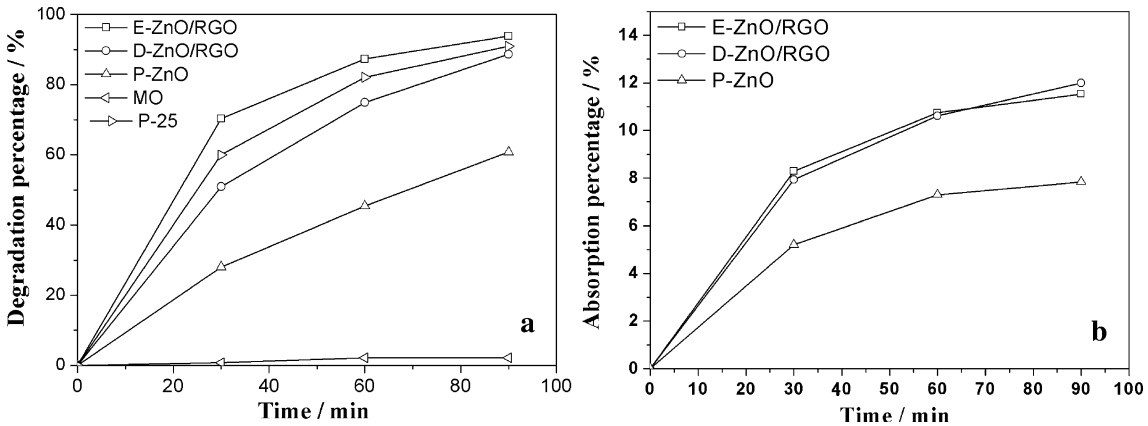

Fig. 5 UV photocatalytic degradation (**a**) and dark absorption (**b**) of MO for as-prepared samples

30th min. The result was compared with Degussa P25, which is well-known to have a superior photocatalytic activity. E-ZnO/RGO exhibits a higher photocatalytic activity than commercial P25. The values of degradation efficiency at 30th min for E-ZnO and P25 were 70.3 and 59.7%, respectively. It implied that the interaction between RGO and ZnO photocatalyst played a crucial role in the enhancement of photocatalytic activity.

The adsorption properties of the catalysts were tested by putting the suspension in dark circumstance (Fig. 5b). It is true that the absorption property of ZnO/RGO composites was slightly higher than that of pure ZnO but the difference was not so obvious. Although D-ZnO/RGO and E-ZnO/RGO showed similar absorbability, they performed evidently different photocatalytic properties. So we can conclude that a higher absorbability of ZnO/RGO composites is not the main reason for their greater photocatalytic properties.

The recycled experiments for the photodegradation of MO were performed as well, and the results are given in Fig. 6. After 30 h of exposed under UV light, an evident decrease of photocatalytic activity for P-ZnO was found (Fig. 6a), the degradation efficiency within 90 min decreased from 61 to 49%. When it comes to 80 h, only 23% of the MO was degraded within 90 min. Meanwhile, it is much better for E-ZnO/RGO (Fig. 6b) under the same situation, and its photodegradation activity did not apparently affected even after 80 h of irradiation by UV light. Although decreases can be observed at the early stage of photocatalytic process, the degradation efficiencies within 90 min were above 90% for all of them. It is clear that the photocorrosion effect of ZnO was suppressed in ZnO/RGO composites.

As it is well-known that ZnO would decompose and release Zn^{2+} ions under illumination for its photocorrosion effect [25]. To further study the photocorrosion effect, the concentration of Zn^{2+} in the solution was measured with ICP test after exposure for 30, 50, and 80 h, and the results are shown in Fig. 7. Evidently, the concentration of Zn^{2+} for P-ZnO suspension is much higher than that of E-ZnO/RGO, suggesting the photoinduced dissolution of ZnO is effectively prevented in E-ZnO/RGO. The ICP tests were also in good agreement with the results of the circled photochemical experiment.

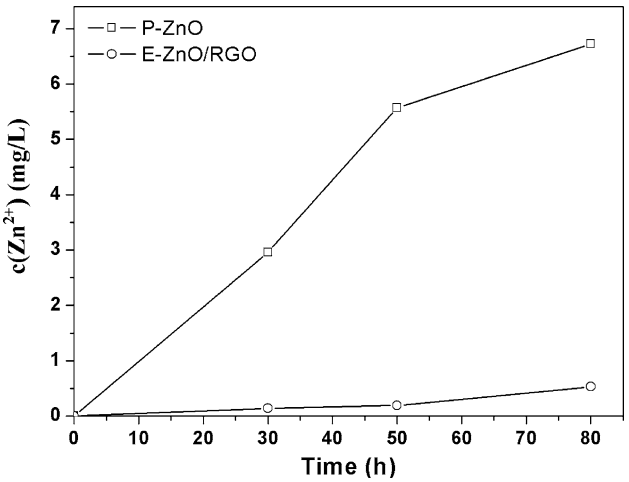

Fig. 7 Concentration of Zn^{2+} induced by the ZnO decomposition under UV light

Discussion

Formation process of ZnO/RGO

The active groups(C=O, –C–O–C–, –C–OH) endow GO with a large surface area and strong ion exchange capacity, which make it possible for Zn^{2+} to enter into the interlayer of GO. And then ZnO nanoparticles can be formed in the interlayer of GO. GO would be reduced at the same time because the groups were consumed during the reactions.

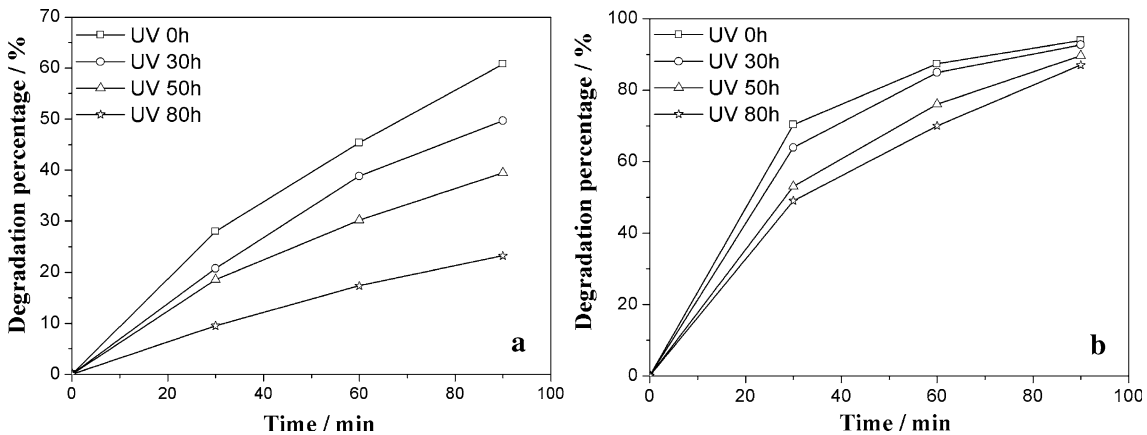

Fig. 6 Recycled experiments of P-ZnO (**a**) and E-ZnO/RGO (**b**)

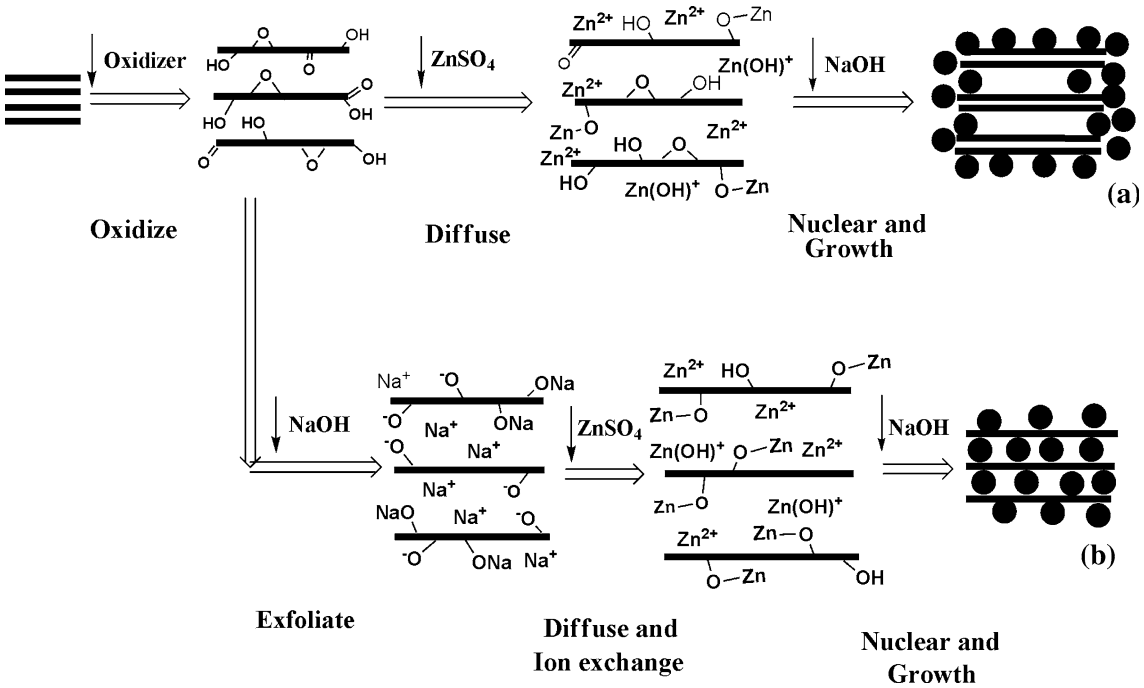

Fig. 8 Formation process of different photocatalysts: **a** D-ZnO/RGO; **b** E-ZnO/RGO

Figure 8a describes the formation process of D-ZnO/RGO. In this situation, diffusion is the predominant manner for Zn^{2+} entering into the interlayer of GO. The diffusion process is hindered by a considerable resistance because the interlayer distance is not large enough. A large amount of Zn^{2+} ions would stay on the external surface and the fringe of interlayer. When NaOH solution is dropped, heterogeneous nucleation in these positions will be prior to the homogeneous in the solution**.** So ZnO nanoparticles are mainly grown in these areas which can be observed in the FE-SEM image (Fig. 3a).

Figure 8b presents the formation process of E-ZnO/RGO. Compared with the D-ZnO/RGO process, the most distinctive difference is the ultrasonic processing of GO with NaOH. Since GO contains acidic hydroxyl groups (such as C=O, –C–O–C–, –C–OH), C–O^- could be formed in GO layers when GO is neutralized by dilute alkaline solution, and Na^+ ions would take the place of H^+ at the same time. The bigger diameter of Na^+ and electrostatic repulsive force between C–O^- groups among GO layers cause the formation of exfoliated GO (EGO) [26]. The layers of EGO would be much thinner since its interlayer distance is much larger than that of GO. So far, Zn^{2+} ions would be easier to enter into the interlayer of EGO. Then Zn^{2+} ions bond with C–O^- and followed by the nucleation of ZnO when NaOH is dropped. The sandwich structure is formed together with the nucleation of ZnO because Zn^{2+} ions have already bonded with carbons before. The sandwich structure of E-ZnO/RGO was also well performed in its FE-SEM image (Fig. 3c).

Mechanisms of enhanced-photocatalytic activity and suppression of photocorrosion effect

When ZnO is irradiated by UV light, e^-–h^+ pairs are generated. The e^- and h^+ can migrate to the surface to react with the adsorbed reactants in the desired process, but some can undergo an undesired recombination. A rate increase in the former process or a rate decrease in the latter would lead to greater photocatalytic efficiency.

The main photocatalysis process of ZnO/RGO can be described as follows (Fig. 9): When excited by the UV light, electrons in valence band (VB) can jump to conduction band (CB) and diffuse to the interface of ZnO and RGO. With a good conductivity, RGO could be a good acceptor of photo-induced electrons. Hence the recombination would be

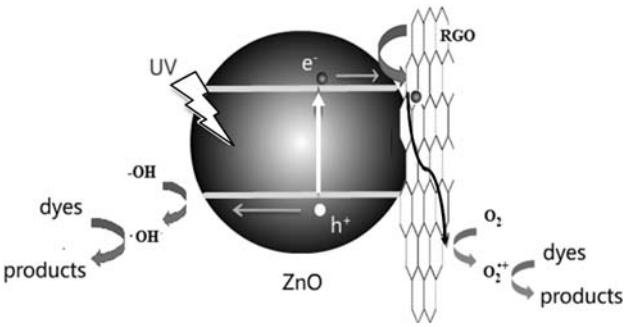

Fig. 9 General mechanism of the photocatalysis of as-prepared ZnO/RGO composites

effectively suppressed and this has been confirmed by the PL analysis before. As a result of this, much more holes (h^+) could diffuse to the surface of ZnO and cause the formation of hydroxyl radicals ($^{\bullet}OH$), which subsequently degrade the MO target. Meanwhile, the transferred electrons might react with dissolved oxygen to form the superoxide radicals ($^{\bullet}O_2^-$), which would also react with the dye molecules. The greatly enhanced-photocalytic activity could be attributed to the above reasons.

Since RGO paves the way for migration of electrons, a better graphitization is expected to have higher electron transfer efficiency and thus have a better photocatalysis activity. So it will be understandable that the photocatalysis activity E-ZnO/RGO is better than that of D-ZnO/RGO.

It is reported that the photocorrosion of ZnO was caused by the surface unsaturated oxygen atoms [11], which would react with holes and escape from the surface. And the reactions of this process can be described as follows [27]:

$$O^{2-}_{surface} + h^+ \rightarrow O^-_{surface} \quad (4)$$

$$O^-_{surface} + 3O^{2-} + 3h^+ \rightarrow 2\left(O - O^{2-}\right) \quad (5)$$

$$\left(O - O^{2-}\right) + 2h^+ \rightarrow O_2 \quad (6)$$

$$2Zn^{2+} \rightarrow 2Zn^{2+}(aq) \quad (7)$$

The overall reaction may be represented as

$$ZnO + 2\,h^+ \rightarrow Zn^{2+} + 0.5O_2 \quad (8)$$

The loss of oxygen not only consumed the holes but also caused the Zn^{2+} to dissolve from ZnO and followed by a damage of the crystal structure, which would inevitably weaken the photocatalytic activity of ZnO. When ZnO was hybridized with RGO, a combination would be formed between RGO the surface unsaturated oxygen atoms of ZnO. Consequently, the number of surface unsaturated oxygen atoms could be sharply decreased. Therefore holes would prefer to react with dyes instead of performing the reaction 4 and the photocorrosion of ZnO could be effectively inhibited.

Conclusions

Sandwich-structured ZnO/RGO composites were successfully prepared by different means at relatively low temperature (60 °C). Ultrasonic processing of GO with NaOH could further enlarge the interlayer distance of GO, which makes it easy for Zn^{2+} to move into the interlayer of GO and followed by the formation of more regular-layered structure.

During the formation of ZnO/RGO composites, GO was reduced to graphite-like carbon (RGO), the good conductivity of which paved a way for the transfer of photo-induced electrons. The migration photo-induced electrons could take place on the interface of RGO and ZnO, which effectively suppressed the recombination of e^-–h^+ pair. As a result, the UV photocatalytic activity would be greatly enhanced.

When RGO was introduced, the surface unsaturated oxygen atoms of ZnO could combine with RGO, which prevented the surface oxygen atoms and Zn^{2+} from escaping from ZnO nanoparticles and then the photocorrosion of ZnO was effectively inhibited.

Acknowledgements This research was supported by the National Natural Science Foundation of China (Grant Number 50672066).

References

1. Petra N, Jirı Z, Josef K, Vıt K, Jirı R (2007) Appl Catal B 79:179
2. Idoko JO, Oluwapomile OO, Robert PF, Steve P, Alison W, Joseph W, Mike Winterbottom J (2007) Catal Today 128:100
3. Euvananont C, Junin C, Inpor K, Limthongkul P, Thanachayanont C (2008) Ceram Int 34:1067
4. Xiaodong Z, Haijia S, Yan Z, Tianwei T (2008) J Photochem Photobiol A 199:123
5. Bircan D, Siddik I (2001) J Photochem Photobiol A 140:263
6. Yeber MC, Roderiguez J, Freer J, Baeza J, Duran N, Mansilla HD (1999) Chemosphere 39:1679
7. Serpone N, Maruthamuthu P, Pichat P, Pelizzetti E, Hidaka H (1995) J Photochem Photobiol A 85:247
8. Amina AK, Tahar S, Jean-François P, Pierre B (2001) J Photochem Photobiol A 141:231
9. Narayanasamy S, Manickavasakam M, Meenakshisundaram S (2008) Catal Commun 9:262
10. Byrappa K, Dayananda AS, Sajan CP, Basavalingu B, Shayan MB, Soga K, Yoshimura M (2008) J Mater Sci 43:2348. doi: 10.1007/s10853-007-1989-8
11. Hongbo F, Tongguang X, Shengbao Z, Yongfa Z (2008) Environ Sci Technol 42:8064
12. Tamas S, Otto B, Imre D (2005) Carbon 43:3181
13. Hae KJ, Leyla C, Mei HJ, Per AG, Kevin ES, Young HL (2008) Chem Phys Lett 460:499
14. Lerf A, Buchsteiner A, Pieper J, Schottl S, Dekany I, Szabo T, Boehm HP (2006) J Phys Chem Solids 67:1106
15. Hummers WS Jr, Offeman RE (1958) J Am Chem Soc 80(6):1339
16. Tamas S, Etelka T, Erzsebet I, Imre D (2006) Carbon 44:537
17. Han Y, Lu Y (2008) Synth Met 158(19–20):744
18. Jiayan X, Yuan H, Lei S, Qingan W, Weicheng F (2002) Carbon 40:2961
19. Xiao P, Xiao M, Liu PG, Gong KC (2000) Carbon 38:623
20. Satoshi Y, Hiroaki I (2002) J Mater Chem 12:3773
21. Tetsuo K, Hiroaki I (2005) J Cryst Growth 283:490
22. Yinhong Z, Yunqiu H (2007) Front Mater Sci China 1(3):297
23. Reenamole G, Michael KS, Suresh CP (2008) J Phys Chem C 112:13563
24. Xu F, Yuan Z-Y, Du G-H, Halasa M, SU B-L (2007) Appl Phys A 86:181
25. Domenech J, Prieto A (1986) J Phys Chem 90(6):1123
26. Matsuo Y, Hatase K, Sugie Y (1997) Carbon 35:113
27. Rudd AL, Berslin CB (2000) Electrochim Acta 45:1571